Open access • Journal Article • DOI:10.1021/JACS.9B11446

MXene Derived Metal–Organic Frameworks — Source link

Hao Wu, Maram Almalki, Xiangming Xu, Yongjiu Lei ...+7 more authors

Institutions: King Abdullah University of Science and Technology

Published on: 11 Dec 2019 - Journal of the American Chemical Society (American Chemical Society (ACS))

JACS
JOURNAL OF THE AMERICAN CHEMICAL SOCIETY

Communication

pubs.acs.org/JACS

MXene Derived Metal−Organic Frameworks

Hao Wu,[†] Maram Almalki,[‡] Xiangming Xu,[†] Yongjiu Lei,[†] Fangwang Ming,[†] Arijit Mallick,[‡] Vladimir Roddatis,[§] Sergei Lopatin,[∥] Osama Shekhah,[‡] Mohamed Eddaoudi,*[,‡] and Husam N. Alshareef*[,†]

[†]Materials Science and Engineering, Physical Science and Engineering Division, King Abdullah University of Science and Technology (KAUST), Thuwal 23955-6900, Saudi Arabia

[‡]Advanced Membranes and Porous Materials Center, Physical Science and Engineering Division, Functional Materials Design, Discovery and Development (FMD3), King Abdullah University of Science and Technology (KAUST), Thuwal 23955-6900, Saudi Arabia

[§]Interface Geochemistry, German Research Centre for Geosciences, GFZ, Telegrafenberg, 14473 Potsdam, Germany

[∥]King Abdullah University of Science and Technology (KAUST), Core Laboratories, Thuwal 23955-6900, Saudi Arabia

Supporting Information

ABSTRACT: Synthesis of nanoscale metal−organic frameworks (MOFs) is a highly challenging task because conventional soluble metal salt precursors are not easy to manipulate spatially, thus normally leading to bulk MOFs. In the present work, V_2CT_x MXene is demonstrated for the first time as a metal precursor to fabricate two-dimensional (2D) MOF nanosheets, whose thickness (6 to 18 nm) can be tuned by varying the reaction temperature. The highly electronegative surface atoms of MXene and sufficient accessible attacking sites for ligands are responsible for the evolution of 2D MOF nanosheets. Moreover, highly oriented and smooth MOF thin films have been grown based on these nanosheets using a convenient spin coating process. With the impregnation of nonvolatile H_3PO_4, the MOF thin film exhibits a proton-conducting property. This study demonstrates that high-quality 2D MOF sheets and thin films are enabled by 2D MXene precursors. We believe that the high-quality MOF films prepared in this study pave the way for many device applications.

Metal−organic frameworks (MOFs) have attracted enormous attention in versatile research fields such as gas storage/separation, sensing, catalysis, etc., thanks to their inherent porosity, large surface area, and numerous structural and chemical tunability.[1−5] However, manipulating conventional bulk MOFs into 2D nanosheets and thin-film form is very challenging, but extremely significant. This is because such MOF morphologies can enable new applications in electronics, sensors, and other device applications.[6−11] In pursuit of MOF thin films, layer-by-layer and Langmuir−Blodgett techniques have been developed.[12−14] Yet, these protocols require specific surface topologies and/or interfaces, specialized equipment, and skilled multistep operations, which severely restrict their large-scale practical applications.[15−17] Alternatively, tailoring MOFs themselves into the nanoscale with controlled growth dimensionalities (e.g., two-dimensional, 2D) and architectures is highly desirable, as they, beyond the bulk MOFs, could meet the specific requirements to those areas.[18−25]

In general, MOFs are constructed by coordination reactions between soluble inorganic metal salts (e.g., nitrates, chlorides, and acetates) and organic ligands in polar solvents.[26,27] However, using conventional MOF synthesis methods, one typically has little control over the construction of MOFs with the desired dimensionality. In pursuit of the well-defined geometrical shape of MOF crystals, eco-friendly and cost-effective insoluble metal precursors (e.g., metals, metal oxides/hydroxides) have been developed.[28−34] Among them, some are used as hard templates while some serve simultaneously as sacrificial templates where the parental features could be readily inherited. Yet, the hard template approach is restricted in wide utilization due to the fact that the precursors are normally anchored on substrates. In addition, incomplete conversion of metal residuals has been observed, leading to inseparable MOF/metal composite species.[34] Recently, Moran and coauthors have demonstrated an insoluble metal carbide (Al_4C_3) precursor to prepare needle-like MIL-53 (Al) MOF crystals.[27] However, the low surface area of the bulk precursor provided limited accessible sites to spatially control the nucleation to form mesoscopic architectures.

MXenes are an emerging group of 2D laminated inorganic transition metal carbides, nitrides, or carbonitrides with a general formula of $M_{n+1}X_nT_x$ (n = 1−3), where M represents early transition metals (e.g., Ti, V, etc.), X is C and/or N, and T_x is surface terminations (−F, −O, and −OH).[35−39] To date, over 30 MXenes with wide chemical and structural varieties have been synthesized.[38] Notably, the terminal atoms on the surface of MXene, having low work function and high electronegativity,[39] enable them to be strong electron acceptors, which is beneficial for the deprotonation of organic ligands and thus the subsequent bridging with the underlying metal atoms. Meanwhile, the sufficient accessible surfaces of the atomically thin 2D MXene could provide adequate attack sites

Received: October 24, 2019
Published: December 11, 2019

DOI: 10.1021/jacs.9b11446
J. Am. Chem. Soc. XXXX, XXX, XXX−XXX

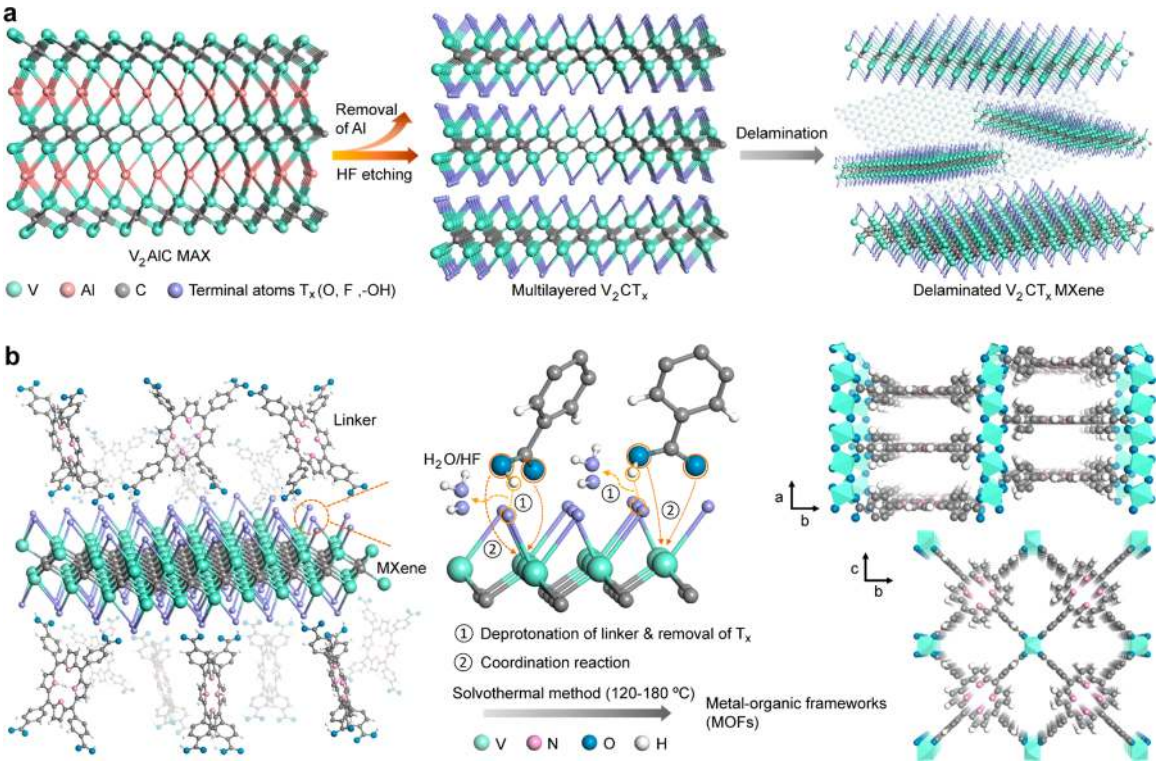

Figure 1. Scheme showing the preparation of (a) V_2CT_x MXene, and (b) V_2CT_x MXene-derived MOF (V_2CT_x-PMOF).

for the protonated ligands, which could accelerate the reaction while preserving the underlying 2D topology.

Herein, we have demonstrated for the first time that MXene can be employed as a metal source for the synthesis of MOFs. As a proof-of-concept, using V_2CT_x MXene and H_2TCPP (H_2TCPP = meso-tetra(4-carboxyl-phenyl) porphyrin) ligand, a novel MOF with a 2D nanosheet morphology (V-PMOF, an analog of Al-PMOF)[40] was obtained. The V_2CT_x MXene was synthesized first by etching Al layers followed with a delamination procedure by TMAOH (TMAOH = tetramethylammonium hydroxide) intercalation (Figure 1a). Then, a facile solvothermal method was employed to convert the V_2CT_x MXene and H_2TCPP into V-PMOF (Figure 1b). The H_2TCPP ligand was selected because it contains a large planar aromatic ring, which may show good topology compatibility with the 2D MXene. Moreover, the protons of carboxylic groups could provide attacking sites for binding the surface atoms of MXene. Additionally, N atoms embraced by the porphyrin core could serve as acceptors of hydrogen bonds to bridge guest molecules (e.g., nonvolatile H_3PO_4), which could afford MOFs with proton-conducting properties.[41] Delightfully, the as-prepared V_2CT_x-PMOF nanosheet could readily stack to form oriented thin films simply by spin coating. Such MOF thin films with guest acid dopants showed proton conductivity, which makes them promising in thin-film electronic, photonic, and sensor devices.[41−46]

A typical accordion-like nanostructure is observed after etching the Al layers out of the densely packed MAX phase (V_2AlC),[47] as depicted in the scanning electron microscopy (SEM) images (Figure S1). The X-ray diffraction (XRD) pattern of MXene indicates a layered feature after delamination (Figure 2a), in accordance with the previous results.[48] The corresponding interlayer spacing is ~1.21 nm, which is much higher than its parental MAX parent phase (~0.65 nm),

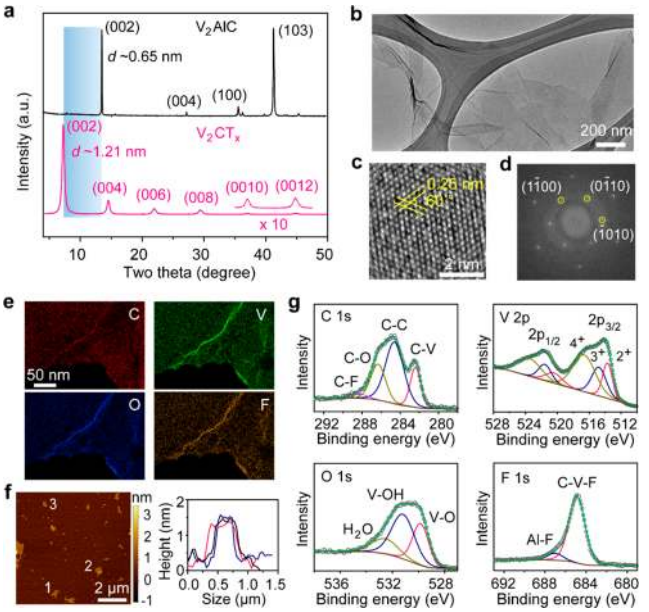

Figure 2. Characterizations of V_2CT_x MXene. (a) XRD patterns. (b−d) TEM, HRTEM images, and fast Fourier transform (FFT) pattern, respectively. (e) EDX mapping. (f) AFM image and height profile. (g) XPS spectra.

demonstrating the successful synthesis of 2D MXene. A transmission electron microscopy (TEM) image reveals an ultrathin sheet-like morphology (Figure 2b). A high-resolution TEM (HRTEM) image and corresponding fast Fourier transform (FFT) pattern display the hexagonal symmetry of MXene, perpendicular to the (0010) planes (Figure 2c,d). Additionally, energy-dispersive X-ray (EDX) elemental mapping manifested that all elements are distributed homoge-

DOI: 10.1021/jacs.9b11446
J. Am. Chem. Soc. XXXX, XXX, XXX−XXX

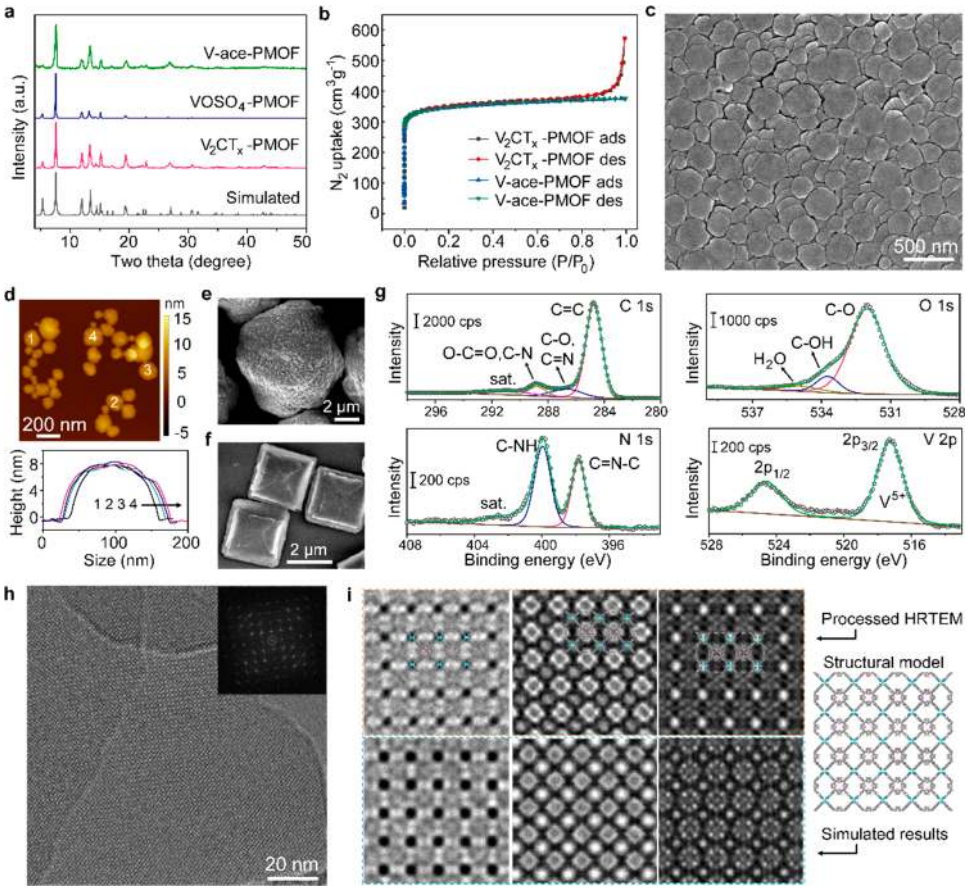

Figure 3. Characterizations of MOFs. (a) XRD patterns of V_2CT_x MXene, $VOSO_4$, and Vanadium acetate-derived PMOFs (denoted as V_2CT_x-PMOF, $VOSO_4$-PMOF, and V-ace-PMOF, respectively) and simulated result. (b) N_2 isotherms of V_2CT_x-PMOF and V-ace-PMOF. (c) SEM image of V_2CT_x-PMOF. (d) AFM image and height profiles of V_2CT_x-PMOF (150 °C). (e, f) SEM images of $VOSO_4$-PMOF and V-ace-PMOF, respectively. (g) XPS spectra of V_2CT_x-PMOF. (h) TEM image of V_2CT_x-PMOF. Inset, FFT pattern. (i) Processed HRTEM images by real-space averaging (upper) and simulated results (down) of V_2CT_x-PMOF. The simulation conditions are −405 nm, +220 nm, and +140 nm defocus (left to right), respectively.

neously in the nanosheets (Figure 2e). The thickness of the nanosheets detected by atomic force microscopy (AFM) is around 1.2 nm, implying the formation of V_2CT_x monolayers (Figure 2f). High-resolution X-ray photoelectron spectroscopy (XPS) analysis of MXene was performed to investigate the terminal atomic bonding (Figure 2g and Figure S2), where the atomic ratio of V (45.9%) to C (21.7%) is close to 2, which is in agreement with the stoichiometric proportion of V_2CT_x. Quantitative terminal O (16.8%) and F (15.7%) atoms were further verified in the V_2CT_x MXene.[47−49]

The feasibility of using V_2CT_x MXene as metal sources to synthesize MOFs was tested via the solvothermal reaction with H_2TCPP and is confirmed by XRD (Figure 3a). Both the V_2CT_x MXene and other soluble metal salts ($VOSO_4$ and vanadium acetate)-derived powders show excellent agreement with the simulated result.[40] This is also applied to other carboxyl acid containing ligands (e.g., terephthalic acid, Figure S3), suggesting the universality of V_2CT_x MXene as metal sources in MOF synthesis. The porosity of V_2CT_x-PMOF and V-ace-PMOF were investigated, and they both exhibit a type-I N_2 sorption isotherms (Figure 3b). The experimental Brunauer−Emmett−Teller (BET) surface areas are 1397 and 1357 $m^2\ g^{-1}$ respectively, indicating the complete conversion of MXene to MOF. SEM images of the V_2CT_x-PMOF display a 2D sheet-like morphology with lateral sizes ranging from one hundred to few hundreds of nanometers (Figure 3c and Figure S4). Meanwhile the thickness of the V_2CT_x-PMOF sheets can be tuned from 6 to 18 nm by varying the reaction temperature (120 to 180 °C, Figure 3d and Figure S5). The reaction intermediates show both MOF nanosheets and cracked MXenes, implying a dissolution−reprecipitation formation mechanism (Figure S6). In comparison, the $VOSO_4$-PMOF and V-ace-PMOF show a much larger spherical (>10 μm) and cubic (>2 μm) structure, respectively (Figure 3e, f). The nanosheet morphology is not attainable when using the multilayered V_2CT_x either, which might be due to the limited accessible sites (Figure S7). XPS analysis of the V_2CT_x-PMOF showed that the bonds of MXene (V−C and V−F) have disappeared, while aromatic C═C and C−O bonds originating from the TCPP ligands became dominant (Figure 3g). The atomic ratio of N (5.1%) to V (1.5%) is in accordance with that of the EDX result (Figures S8, S9), implying ∼2.8 DMF molecules per unit in the V_2CT_x-PMOF, which is consistent with previously reported results.[40] Moreover, two distinct peaks (C−NH and C═N−C) were deconvoluted from the N 1s spectrum, implying that no V was located at the center of the porphyrin rings. This was confirmed by the UV−visible absorption spectrum (Figure S10), where four Q bands at lower binding energies are observed due to $\pi-\pi^*$ transitions in the free-base porphyrins.[40,50] Additionally, Fourier transform

DOI: 10.1021/jacs.9b11446
J. Am. Chem. Soc. XXXX, XXX, XXX−XXX

infrared spectroscopy shows the N−H stretching vibration (3320 cm^{-1}) and in-plane vibration (964 cm^{-1}) peaks (Figure S11), further indicating nonmetalated centers.[50] More directly, the crystal structure of V_2CT_x-PMOF was captured using low-dose HRTEM (by which the beam-sensitive structure could be imaged at the atomic level).[51,52] Figure 3h shows a typical HRTEM image that was taken along the ⟨100⟩ zone axis, where highly ordered cages are observed (consistent with that of V-ace-PMOF, Figure S12). The corresponding FFT shows a cubic structural feature, which is consistent with the crystal structure of V_2CT_x-PMOF. Moreover, the processed HRTEM images present a good match with the projected structural model and simulated results (see raw images in Figure S13 and simulation details). Normally, it is highly challenging to capture the crystal structures of 2D MOFs at atomic resolution. The good preservation of the original crystal structure implies its decent stability. Thermogravimetric analysis reveals that the V_2CT_x-PMOF nanosheets are stable up to 350 °C in a nitrogen atmosphere (Figure S14).

The nanosheet morphology of the synthesized V_2CT_x-PMOF inspired us to explore their fabrication as thin films, which could open the door for many applications. A simple spin-coating strategy was adopted to fabricate MOF thin films using a suspension (Figure S15, 1 mg mL^{-1}). As presented in Figure 4a−d, MOF thin films can be constructed on both glasses and flexible plastic substrates with a root-mean-square roughness of ∼9.5 nm and a thickness of ∼20 nm while retaining good transparency. UV−vis transmission spectroscopy indicates that the thin films have an obvious peak at around 420 nm, in correspondence with the absorption spectrum, while a high transmittance (75% and 60%, respectively) after 500 nm is observed (Figure 4e). Interestingly, the XRD of the thin film features sharp (*l*00) peaks with almost no additional reflections, which fits with the simulated result along the ⟨100⟩ direction (Figure 4f), indicating the highly oriented stacking of the V_2CT_x-PMOF nanosheets. Note that the fabrication of MOF thin films using the spin coating process (especially with a specific orientation) is rare and difficult. Such thin films are not achievable using PMOFs derived from the other two precursors, implying the uniqueness and superiority of MXene-derived PMOFs. As the center of porphyrin rings are not metalated, the inner N atoms could serve as acceptors of hydrogen bonds. Thus, nonvolatile H_3PO_4 enables the solid MOF thin films with a potent proton-conducting property by forming hydrogen bond networks within the MOFs. The protonation of N after acid impregnation can be confirmed by the color change (Figure S16) and the red-shifted peaks of Q bands in the UV−visible absorption spectrum (Figure 4g).[50] The XRD pattern shows a slightly left-shifted (200) peak, which might be induced by the stronger charge repulsion between the proton-doped porphyrin centers after acid-doping (Figure S17). Alternating-current impedance measurements were performed on the MOF thin film using interdigitated electrodes at varying temperature (Figure S18). The proton conductivity ranged from 2.76 to 7.96 × 10^{-4} S cm^{-1} with an activation energy of 0.15 eV (Figure 4h), indicating that the acid-doped MOF thin film follows the Grotthus mechanism which initiates the proton conducting through hydrogen-bond networks.[41−46]

In summary, we developed MXene as a new metal source for the synthesis of MOFs. The highly electronegative terminal atoms and adequate accessible surfaces of the MXene enable the topological synthesis and fabrication to MOFs with 2D nanosheet morphology. The as-prepared V_2CT_x-PMOF with 2D nanosheets with tunable thickness could stack in a specific orientation to form thin films. The MOF thin films exhibited exceptional uniformity, which is superior to previously reported MOF thin films. These V_2CT_x-PMOF exhibited appealing proton conductivity with acid impregnation, which is promising in electronic, sensing, and electrochemical applications.

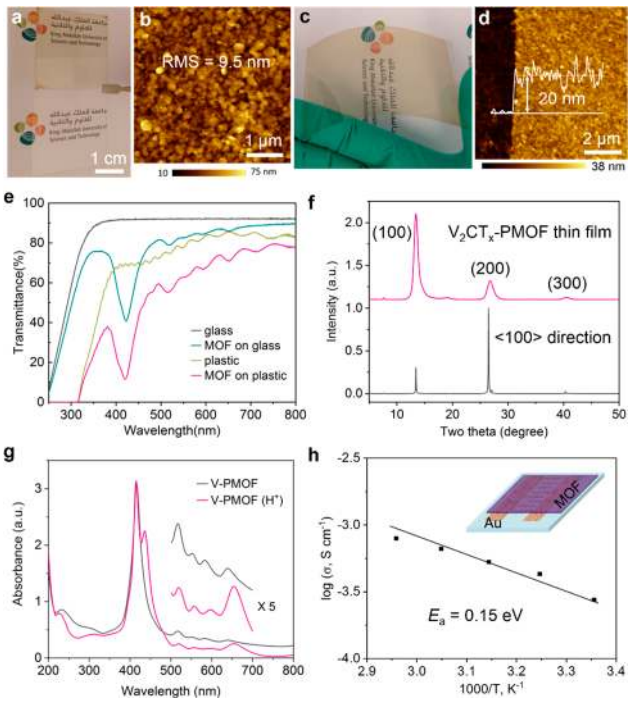

Figure 4. Characterizations of V_2CT_x-PMOF thin films. (a, b) V_2CT_x-PMOF thin film on glass substrate and corresponding AFM image. (c, d) V_2CT_x-PMOF thin film on plastic substrate and corresponding AFM image. (e) UV−vis transmittance of V_2CT_x-PMOF thin films. (f) XRD pattern of V_2CT_x-PMOF thin film and simulated diffraction result along ⟨100⟩ direction. (g) UV−vis absorption spectra with and without phosphoric acid dopants of V_2CT_x-PMOF. (h) Arrhenius plot of acid-doped V_2CT_x-PMOF thin film. Inset, the model for test.

■ ASSOCIATED CONTENT

Supporting Information

The Supporting Information is available free of charge at https://pubs.acs.org/doi/10.1021/jacs.9b11446.

Experimental details for MXene and MOFs synthesis, HRTEM acquisition and simulation, proton conductivity measurement, SEM, XPS, XRD, AFM, UV−vis absorption, FTIR, HRTEM, Thermogravimetric analysis, optical image, Nyquist plots (PDF)

■ AUTHOR INFORMATION

Corresponding Authors

*mohamed.eddaoudi@kaust.edu.sa

*husam.alshareef@kaust.edu.sa

ORCID

Yongjiu Lei: 0000-0003-1663-6102

Fangwang Ming: 0000-0003-4574-9720

Sergei Lopatin: 0000-0003-3916-3803

Osama Shekhah: 0000-0003-1861-9226

DOI: 10.1021/jacs.9b11446
J. Am. Chem. Soc. XXXX, XXX, XXX−XXX

Mohamed Eddaoudi: 0000-0003-1916-9837
Husam N. Alshareef: 0000-0001-5029-2142

Notes

The authors declare no competing financial interest.

■ ACKNOWLEDGMENTS

This work was financially supported by King Abdullah University of Science and Technology (KAUST) under Award No. OSR-CRG2017-3379.

■ REFERENCES

(1) Han, X.; Godfrey, H. G. W.; Briggs, L.; Davies, A. J.; Cheng, Y.; Daemen, L. L.; Sheveleva, A. M.; Tuna, F.; McInnes, E. J. L.; Sun, J.; Drathen, C.; George, M. W.; Ramirez-Cuesta, A. J.; Thomas, K. M.; Yang, S.; Schroder, M. Reversible adsorption of nitrogen dioxide within a robust porous metal-organic framework. *Nat. Mater.* **2018**, *17*, 691−696.

(2) Gong, X.; Noh, H.; Gianneschi, N. C.; Farha, O. K Interrogating Kinetic versus Thermodynamic Topologies of Metal-Organic Frameworks via Combined Transmission Electron Microscopy and X-ray Diffraction Analysis. *J. Am. Chem. Soc.* **2019**, *141*, 6146−6151.

(3) Zhang, L.; Yuan, S.; Feng, L.; Guo, B.; Qin, J. S.; Xu, B.; Lollar, C.; Sun, D.; Zhou, H. C. Pore-Environment Engineering with Multiple Metal Sites in Rare-Earth Porphyrinic Metal-Organic Frameworks. *Angew. Chem., Int. Ed.* **2018**, *57*, 5095−5099.

(4) Kim, H.; Yang, S.; Rao, S. R.; Narayanan, S.; Kapustin, E. A.; Furukawa, H.; Umans, A. S.; Yaghi, O. M.; Wang, E. N. Water Harvesting from Air with Metal-Organic Frameworks Powered by Natural Sunlight. *Science* **2017**, *356*, 430−434.

(5) Mallick, A.; El-Zohry, A. M.; Shekhah, O.; Yin, J.; Jia, J.; Aggarwal, H.; Emwas, A. H.; Mohammed, O. F.; Eddaoudi, M. Unprecedented Ultralow Detection Limit of Amines using a Thiadiazole-Functionalized Zr(IV)-Based Metal-Organic Framework. *J. Am. Chem. Soc.* **2019**, *141*, 7245−7249.

(6) Yoon, S. M.; Park, J. H.; Grzybowski, B. A. Large-Area, Freestanding MOF Films of Planar, Curvilinear, or Micropatterned Topographies. *Angew. Chem., Int. Ed.* **2017**, *56*, 127−132.

(7) Xu, G.; Yamada, T.; Otsubo, K.; Sakaida, S.; Kitagawa, H. Facile "Modular Assembly" for Fast Construction of a Highly Oriented Crystalline MOF Nanofilm. *J. Am. Chem. Soc.* **2012**, *134*, 16524−16527.

(8) Hu, A.; Pang, Q.; Tang, C.; Bao, J.; Liu, H.; Ba, K.; Xie, S.; Chen, J.; Chen, J.; Yue, Y.; Tang, Y.; Li, Q.; Sun, Z. Epitaxial Growth and Integration of Insulating Metal-Organic Frameworks in Electrochemistry. *J. Am. Chem. Soc.* **2019**, *141*, 11322−11327.

(9) Liu, J.; Woll, C. Surface-Supported Metal-Organic Framework Thin Films: Fabrication Methods, Applications, and Challenges. *Chem. Soc. Rev.* **2017**, *46*, 5730−5770.

(10) Zhao, M.; Lu, Q.; Ma, Q.; Zhang, H. Two-Dimensional Metal-Organic Framework Nanosheets. *Small Methods* **2017**, *1*, 1600030.

(11) Zhao, M.; Wang, Y.; Ma, Q.; Huang, Y.; Zhang, X.; Ping, J.; Zhang, Z.; Lu, Q.; Yu, Y.; Xu, H.; Zhao, Y.; Zhang, H. Ultrathin 2D Metal-Organic Framework Nanosheets. *Adv. Mater.* **2015**, *27* (45), 7372−7378.

(12) Makiura, R.; Motoyama, S.; Umemura, Y.; Yamanaka, H.; Sakata, O.; Kitagawa, H. Surface Nano-architecture of a Metal-Organic Framework. *Nat. Mater.* **2010**, *9*, 565−571.

(13) Motoyama, S.; Makiura, R.; Sakata, O.; Kitagawa, H. Highly Crystalline Nanofilm by Layering of Porphyrin Metal-Organic Framework Sheets. *J. Am. Chem. Soc.* **2011**, *133*, 5640−5643.

(14) Liu, J.; Shekhah, O.; Stammer, X.; Arslan, H. K.; Liu, B.; Schüpbach, B.; Terfort, A.; Wöll, C. Deposition of Metal-Organic Frameworks by Liquid-Phase Epitaxy: The Influence of Substrate Functional Group Density on Film Orientation. *Materials* **2012**, *5*, 1581−1992.

(15) Moreno-Moreno, M.; Troyano, J.; Ares, P.; Castillo, O.; Nijhuis, C. A.; Yuan, L.; Amo-Ochoa, P.; Delgado, S.; Gomez-Herrero, J.; Zamora, F.; Gomez-Navarro, C. One-Pot Preparation of Mechanically Robust, Transparent, Highly Conductive, and Memristive Metal-Organic Ultrathin Film. *ACS Nano* **2018**, *12*, 10171−10177.

(16) Pustovarenko, A.; Goesten, M. G.; Sachdeva, S.; Shan, M.; Amghouz, Z.; Belmabkhout, Y.; Dikhtiarenko, A.; Rodenas, T.; Keskin, D.; Voets, I. K.; Weckhuysen, B. M.; Eddaoudi, M.; de Smet, L.; Sudholter, E. J. R.; Kapteijn, F.; Seoane, B.; Gascon, J. Nanosheets of Nonlayered Aluminum Metal-Organic Frameworks through a Surfactant-Assisted Method. *Adv. Mater.* **2018**, *30*, 1707234.

(17) Virmani, E.; Rotter, J. M.; Mahringer, A.; von Zons, T.; Godt, A.; Bein, T.; Wuttke, S.; Medina, D. D. On-Surface Synthesis of Highly Oriented Thin Metal-Organic Framework Films through Vapor-Assisted Conversion. *J. Am. Chem. Soc.* **2018**, *140*, 4812−4819.

(18) Sheberla, D.; Bachman, J. C.; Elias, J. S.; Sun, C. J.; Shao-Horn, Y.; Dinca, M. Conductive MOF Electrodes for Stable Supercapacitors with High Areal Capacitance. *Nat. Mater.* **2017**, *16*, 220−224.

(19) Feng, D.; Lei, T.; Lukatskaya, M. R.; Park, J.; Huang, Z.; Lee, M.; Shaw, L.; Chen, S.; Yakovenko, A. A.; Kulkarni, A.; Xiao, J.; Fredrickson, K.; Tok, J. B.; Zou, X.; Cui, Y.; Bao, Z. Robust and Conductive Two-Dimensional Metal-Organic Frameworks with Exceptionally High Volumetric and Areal Capacitance. *Nat. Energy* **2018**, *3*, 30−36.

(20) Yang, C.; Dong, R.; Wang, M.; Petkov, P. S.; Zhang, Z.; Wang, M.; Han, P.; Ballabio, M.; Brauninger, S. A.; Liao, Z.; Zhang, J.; Schwotzer, F.; Zschech, E.; Klauss, H. H.; Canovas, E.; Kaskel, S.; Bonn, M.; Zhou, S.; Heine, T.; Feng, X. A Semiconducting Layered Metal-Organic Framework Magnet. *Nat. Commun.* **2019**, *10*, 3260.

(21) Huang, X.; Li, H.; Tu, Z.; Liu, L.; Wu, X.; Chen, J.; Liang, Y.; Zou, Y.; Yi, Y.; Sun, J.; Xu, W.; Zhu, D. Highly Conducting Neutral Coordination Polymer with Infinite Two-Dimensional Silver-Sulfur Networks. *J. Am. Chem. Soc.* **2018**, *140*, 15153−15156.

(22) Zou, L.; Hou, C. C.; Liu, Z.; Pang, H.; Xu, Q. Superlong Single-Crystal Metal-Organic Framework Nanotubes. *J. Am. Chem. Soc.* **2018**, *140*, 15393−15401.

(23) Zhao, S.; Wang, Y.; Dong, J.; He, C.-T.; Yin, H.; An, P.; Zhao, K.; Zhang, X.; Gao, C.; Zhang, L.; Lv, J.; Wang, J.; Zhang, J.; Khattak, A. M.; Khan, N. A.; Wei, Z.; Zhang, J.; Liu, S.; Zhao, H.; Tang, Z. Ultrathin Metal-Organic Framework Nanosheets for Electrocatalytic Oxygen Evolution. *Nat. Energy* **2016**, *1*, 16184.

(24) Ahrenholtz, S. R.; Epley, C. C.; Morris, A. J. Solvothermal Preparation of an Electrocatalytic Metalloporphyrin MOF Thin Film and Its Redox Hopping Charge-Transfer Mechanism. *J. Am. Chem. Soc.* **2014**, *136*, 2464−72.

(25) Wu, H.; Zhang, W.; Kandambeth, S.; Shekhah, O.; Eddaoudi, M.; Alshareef, H. N. Conductive Metal-Organic Frameworks Selectively Grown on Laser-Scribed Graphene for Electrochemical Microsupercapacitors. *Adv. Energy Mater.* **2019**, *9*, 1900482.

(26) Yuan, S.; Feng, L.; Wang, K.; Pang, J.; Bosch, M.; Lollar, C.; Sun, Y.; Qin, J.; Yang, X.; Zhang, P.; Wang, Q.; Zou, L.; Zhang, Y.; Zhang, L.; Fang, Y.; Li, J.; Zhou, H. C. Stable Metal-Organic Frameworks: Design, Synthesis, and Applications. *Adv. Mater.* **2018**, *30*, 1704303.

(27) Moran, C. M.; Joshi, J. N.; Marti, R. M.; Hayes, S. E.; Walton, K. S. Structured Growth of Metal-Organic Framework MIL-53(Al) from Solid Aluminum Carbide Precursor. *J. Am. Chem. Soc.* **2018**, *140*, 9148−9153.

(28) Cai, G.; Zhang, W.; Jiao, L.; Yu, S.-H.; Jiang, H.-L. Template-Directed Growth of Well-Aligned MOF Arrays and Derived Self-Supporting Electrodes for Water Splitting. *Chem.* **2017**, *2*, 791−802.

(29) Deng, T.; Lu, Y.; Zhang, W.; Sui, M.; Shi, X.; Wang, D.; Zheng, W. Inverted Design for High-Performance Supercapacitor Via $Co(OH)_2$-Derived Highly Oriented MOF Electrodes. *Adv. Energy Mater.* **2018**, *8*, 1702294.

(30) Li, X.; Liu, S.; Fan, K.; Liu, Z.; Song, B.; Yu, J. MOF-Based Transparent Passivation Layer Modified ZnO Nanorod Arrays for Enhanced Photo-Electrochemical Water Splitting. *Adv. Energy Mater.* **2018**, *8*, 1800101.

DOI: 10.1021/jacs.9b11446
J. Am. Chem. Soc. XXXX, XXX, XXX−XXX

(31) Falcaro, P.; Okada, K.; Hara, T.; Ikigaki, K.; Tokudome, Y.; Thornton, A. W.; Hill, A. J.; Williams, T.; Doonan, C.; Takahashi, M. Centimetre-Scale Micropore Alignment in Oriented Polycrystalline Metal-Organic Framework Films via Heteroepitaxial Growth. *Nat. Mater.* **2017**, *16*, 342−348.
(32) Yao, M. S.; Tang, W. X.; Wang, G. E.; Nath, B.; Xu, G. MOF Thin Film-Coated Metal Oxide Nanowire Array: Significantly Improved Chemiresistor Sensor Performance. *Adv. Mater.* **2016**, *28*, 5229−5234.
(33) Zhan, G.; Zeng, H. C. Alternative Synthetic Approaches for Metal-Organic Frameworks: Transformation from Solid Matters. *Chem. Commun.* **2017**, *53*, 72−81.
(34) Kornienko, N.; Zhao, Y.; Kley, C. S.; Zhu, C.; Kim, D.; Lin, S.; Chang, C. J.; Yaghi, O. M.; Yang, P. Metal-organic frameworks for electrocatalytic reduction of carbon dioxide. *J. Am. Chem. Soc.* **2015**, *137*, 14129−14135.
(35) Velusamy, D. B.; El-Demellawi, J. K.; El-Zohry, A. M.; Giugni, A.; Lopatin, S.; Hedhili, M. N.; Mansour, A. E.; Fabrizio, E. D.; Mohammed, O. F.; Alshareef, H. N. MXenes for Plasmonic Photodetection. *Adv. Mater.* **2019**, *31*, 1807658.
(36) Tu, S.; Ming, F.; Zhang, J.; Zhang, X.; Alshareef, H. N. MXene-Derived Ferroelectric Crystals. *Adv. Mater.* **2019**, *31*, 1806860.
(37) Naguib, M.; Kurtoglu, M.; Presser, V.; Lu, J.; Niu, J.; Heon, M.; Hultman, L.; Gogotsi, Y.; Barsoum, M. W. Two-Dimensional Nanocrystals Produced by Exfoliation of Ti_3AlC_2. *Adv. Mater.* **2011**, *23*, 4248−4253.
(38) Hart, J. L.; Hantanasirisakul, K.; Lang, A. C.; Anasori, B.; Pinto, D.; Pivak, Y.; van Omme, J. T.; May, S. J.; Gogotsi, Y.; Taheri, M. L. Control of MXenes' Electronic Properties through Termination and Intercalation. *Nat. Commun.* **2019**, *10*, 522.
(39) Hu, T.; Li, Z.; Hu, M.; Wang, J.; Hu, Q.; Li, Q.; Wang, X. Chemical Origin of Termination-Functionalized MXenes: $Ti_3C_2T_2$ as a Case Study. *J. Phys. Chem. C* **2017**, *121*, 19254−19261.
(40) Fateeva, A.; Chater, P. A.; Ireland, C. P.; Tahir, A. A.; Khimyak, Y. Z.; Wiper, P. V.; Darwent, J. R.; Rosseinsky, M. J. A Water-Stable Porphyrin-Based Metal-Organic Framework Active for Visible-Light Photocatalysis. *Angew. Chem., Int. Ed.* **2012**, *51*, 7440−7444.
(41) Ponomareva, V. G.; Kovalenko, K. A.; Chupakhin, A. P.; Dybtsev, D. N.; Shutova, E. S.; Fedin, V. P. Imparting High Proton Conductivity to a Metal-Organic Framework Material by Controlled Acid Impregnation. *J. Am. Chem. Soc.* **2012**, *134*, 15640−15643.
(42) Xu, G.; Otsubo, K.; Yamada, T.; Sakaida, S.; Kitagawa, H. Superprotonic Conductivity in a Highly Oriented Crystalline Metal-Organic Framework Nanofilm. *J. Am. Chem. Soc.* **2013**, *135*, 7438−7441.
(43) Mileo, P. G. M.; Adil, K.; Davis, L.; Cadiau, A.; Belmabkhout, Y.; Aggarwal, H.; Maurin, G.; Eddaoudi, M.; Devautour-Vinot, S. Achieving Superprotonic Conduction with a 2D Fluorinated Metal-Organic Framework. *J. Am. Chem. Soc.* **2018**, *140*, 13156−13160.
(44) Ye, Y.; Guo, W.; Wang, L.; Li, Z.; Song, Z.; Chen, J.; Zhang, Z.; Xiang, S.; Chen, B. Straightforward Loading of Imidazole Molecules into Metal-Organic Framework for High Proton Conduction. *J. Am. Chem. Soc.* **2017**, *139*, 15604−15607.
(45) Wei, Y. S.; Hu, X. P.; Han, Z.; Dong, X. Y.; Zang, S. Q.; Mak, T. C. Unique Proton Dynamics in an Efficient MOF-Based Proton Conductor. *J. Am. Chem. Soc.* **2017**, *139*, 3505−3512.
(46) Nguyen, N. T.; Furukawa, H.; Gandara, F.; Trickett, C. A.; Jeong, H. M.; Cordova, K. E.; Yaghi, O. M. Three-Dimensional Metal-Catecholate Frameworks and Their Ultrahigh Proton Conductivity. *J. Am. Chem. Soc.* **2015**, *137* (49), 15394−15397.
(47) Naguib, M.; Halim, J.; Lu, J.; Cook, K. M.; Hultman, L.; Gogotsi, Y.; Barsoum, M. W. New Two-Dimensional Niobium and Vanadium Carbides as Promising Materials for Li-Ion Batteries. *J. Am. Chem. Soc.* **2013**, *135*, 15966−15969.
(48) VahidMohammadi, A.; Mojtabavi, M.; Caffrey, N. M.; Wanunu, M.; Beidaghi, M. Assembling 2D MXenes into Highly Stable Pseudocapacitive Electrodes with High Power and Energy Densities. *Adv. Mater.* **2019**, *31*, 1806931.
(49) Shah, S. A.; Habib, T.; Gao, H.; Gao, P.; Sun, W.; Green, M. J.; Radovic, M. Template-Free 3D Titanium Carbide ($Ti_3C_2T_x$) MXene Particles Crumpled by Capillary Forces. *Chem. Commun.* **2017**, *53*, 400−403.
(50) Zhao, Y.; Cai, X.; Zhang, Y.; Chen, C.; Wang, J.; Pei, R. Porphyrin-Based Metal-Organic Frameworks: Protonation Induced Q Band Absorption. *Nanoscale* **2019**, *11*, 12250−12258.
(51) Li, X.; Wang, J.; Liu, X.; Liu, L.; Cha, D.; Zheng, X.; Yousef, A. A.; Song, K.; Zhu, Y.; Zhang, D.; Han, Y. Direct Imaging of Tunable Crystal Surface Structures of MOF MIL-101 Using High-Resolution Electron Microscopy. *J. Am. Chem. Soc.* **2019**, *141*, 12021−12028.
(52) Liu, L.; Chen, Z.; Wang, J.; Zhang, D.; Zhu, Y.; Ling, S.; Huang, K. W.; Belmabkhout, Y.; Adil, K.; Zhang, Y.; Slater, B.; Eddaoudi, M.; Han, Y. Imaging Defects and Their Evolution in a Metal-Organic Framework at Sub-Unit-Cell Resolution. *Nat. Chem.* **2019**, *11*, 622−628.

DOI: 10.1021/jacs.9b11446
J. Am. Chem. Soc. XXXX, XXX, XXX−XXX